Cell shape and cell-wall organization in Gram-negative bacteria

Kerwyn Casey Huang[a,1], Ranjan Mukhopadhyay[b], Bingni Wen[a], Zemer Gitai[a], and Ned S. Wingreen[a,2]

[a]Department of Molecular Biology, Princeton University, Washington Road, Princeton, NJ 08544-1014; and [b]Department of Physics, Clark University, 950 Main Street, Worcester, MA 01610

Edited by Michael E. Fisher, University of Maryland, College Park, MD, and approved October 14, 2008 (received for review June 4, 2008)

In bacterial cells, the peptidoglycan cell wall is the stress-bearing structure that dictates cell shape. Although many molecular details of the composition and assembly of cell-wall components are known, how the network of peptidoglycan subunits is organized to give the cell shape during normal growth and how it is reorganized in response to damage or environmental forces have been relatively unexplored. In this work, we introduce a quantitative physical model of the bacterial cell wall that predicts the mechanical response of cell shape to peptidoglycan damage and perturbation in the rod-shaped Gram-negative bacterium *Escherichia coli*. To test these predictions, we use time-lapse imaging experiments to show that damage often manifests as a bulge on the sidewall, coupled to large-scale bending of the cylindrical cell wall around the bulge. Our physical model also suggests a surprising robustness of cell shape to peptidoglycan defects, helping explain the observed porosity of the cell wall and the ability of cells to grow and maintain their shape even under conditions that limit peptide crosslinking. Finally, we show that many common bacterial cell shapes can be realized within the same model via simple spatial patterning of peptidoglycan defects, suggesting that minor patterning changes could underlie the great diversity of shapes observed in the bacterial kingdom.

bacterial cell wall | biophysics | elasticity | peptidoglycan | morphology

Bacterial cells come in a wide variety of shapes and sizes (1), with the cell wall being the primary stress-bearing and shape-maintaining element (2, 3). In recent years, cell shape has been shown to play a critical role in regulating the important bacterial functions of attachment, dispersal, motility, polar differentiation, predation, and cellular differentiation (for a review, see ref. 4). Importantly, to achieve cell growth, the cell wall must continuously reorganize, with collateral risks to cell integrity.

In both Gram-negative and Gram-positive bacteria, the cell wall is constructed from the polymer peptidoglycan, a composite of long strands of glycans crosslinked by stretchable peptides. The resulting elastic network protects the cell from lysis (5). Initially, glycans are polymerized as strands of up to 100 disaccharide subunits (6, 7). The steady-state length distribution of glycan strands in *Escherichia coli* is extremely broad, with a mean of ≈20–30 disaccharide units depending on strain, conditions, and growth phase (7, 8), and some strand lengths ranging upwards of 80 units (2). Each disaccharide unit in a glycan strand is synthesized with a covalently linked peptide that can be crosslinked to a peptide emanating from another glycan strand. The orientation of peptide stems winds around each glycan strand (9). A 3D structure of a relaxed dimeric peptidoglycan segment determined by NMR suggests that subsequent peptides are spaced by ≈120° (10). Molecular dynamics simulations suggest that the minimal energy conformation of an oligosaccharide peptidoglycan chain has a peptide rotation angle closer to 90°, with little restriction on rotations of up to 15° (9). The molecular details of glycan strands are conserved among bacteria, and although there is some variation in the biochemistry of crosslinking, the 3D NMR structure of peptidoglycan fragments is relatively insensitive to the type of peptide crosslinks (10). In Gram-negative bacteria, the cell wall is only 1–3 layers thick (11), and in *E. coli* 80% or more of the peptidoglycan exists as a monolayer (12). Consistent with these earlier results, recent electron cryotomography density profile measurements have revealed that the thickness of the cell wall of both *E. coli* and another Gram-negative bacteria *Caulobacter crescentus* is at most 4 nm (13). Popular hypotheses for the organization of the bacterial cell wall (see ref. 14 for a review) have focused on a horizontal orientation of the glycan strands, arranged in hoops around the circumference of the cylinder and crosslinked via longitudinally oriented peptides.

Although the *E. coli* cell wall normally maintains a cylindrical shape during exponential growth (15), the cell shape can be altered either genetically or environmentally. *E. coli* mutants lacking the high molecular-weight PBP2, a transpeptidase, swell up to resemble spheroplasts (16), while cells lacking the low molecular-weight PBPs 5 and 7 are often branched with 3 or more poles (17, 18). During stationary phase, *E. coli* transform to a more spherical shape (19). Wild-type *E. coli* in micron-scale agarose moldings grow in a variety of cell shapes determined by their confinement, and the new cell shape persists after the bacteria are released (20).

The nature of the crosslinked peptidoglycan network is such that bonds must be broken to permit new growth and division (21). The potential for deleterious consequences of peptidoglycan bond breakage has prompted the "make-before-break" hypothesis in which new material is made and inserted into the cell wall before old material is removed (22). However, the need to always make before breaking assumes that the cell wall is highly vulnerable to defects, which has not been established. Indeed, the peptidoglycan density can be reduced by ≈50% by limiting the supply of the specific precursor mesodiaminopimelic acid without any detectable alteration in morphology or growth (23).

To test the robustness of the Gram-negative cell wall to defects and damage and to probe cell-wall organization, we have developed a physical model that extends the existing hypothesis of peptidoglycan as a 2D (single-layer) cell wall with horizontally oriented glycan strands by explicitly incorporating the mechanical properties of the cell wall. Our physical model predicted that a local accumulation of peptide defects would reproducibly result in a cracked cell shape. To verify these predictions, we used an *E. coli* strain sensitive to the antibiotic vancomycin, which disrupts the formation of peptide crosslinks. In the presence of

Author contributions: K.C.H., R.M., Z.G., and N.S.W. designed research; K.C.H. and B.W. performed research; K.C.H. and B.W. contributed new reagents/analytic tools; K.C.H., R.M., B.W., Z.G., and N.S.W. analyzed data; and K.C.H., R.M., Z.G., and N.S.W. wrote the paper.

The authors declare no conflict of interest.

This article is a PNAS Direct Submission.

Freely available online through the PNAS open access option.

[1]Present address: Department of Bioengineering, Stanford University, Stanford, CA 94305.

[2]To whom correspondence should be addressed. E-mail: wingreen@princeton.edu.

This article contains supporting information online at www.pnas.org/cgi/content/full/0805309105/DCSupplemental.

vancomycin, these cells bulge and "crack" in the same manner as the model cell walls. We then used our verified physical model to demonstrate the robustness of the cell wall to large amounts of defects and damage such as might arise during cell growth, including holes in the peptidoglycan large enough to account for the observed porosity of the cell wall. Finally, we demonstrated that crescent, helical, and lemon-shaped model cells, resembling common bacterial shapes, can be generated via parsimonious patterning of peptidoglycan defects.

Results

Modeling the Gram-Negative Cell Wall. To gain insight into the robustness of cell shape, we developed a simple elastic model for the Gram-negative cell wall. For a rod-shaped bacterium such as *E. coli*, we model the cell wall as a single cylindrical layer with the glycan strands oriented around the circumference of the cylinder and crosslinked by peptides, as shown in Fig. 1*A*, with glycans in green and peptides in red. In our model, the relatively unstretchable glycan subunits and relatively stretchable peptide crosslinks are represented as springs that expand from their relaxed lengths to balance the outward force due to the cell's osmotic pressure (see *Materials and Methods* and Fig. 1*A*). In this single-layer model, every other disaccharide unit along the glycan chain has an un-crosslinked peptide oriented perpendicular to the surface. These peptides are not shown in Fig. 1 or supporting information (SI) Fig. S1 and do not help bear the osmotic stress. The orientation of glycans and peptides shown in Fig. 1 has been hypothesized by Höltje *et al.* (2) to match the biochemical evidence for long glycan strands within a single monolayer of peptidoglycan.

An alternative to the glycan "horizontal" orientation on which we focus in this article is a "scaffold" orientation in which the glycan strands are oriented vertically relative to the cell surface (24). However, the observed amount of peptidoglycan in the *E. coli* cell wall appears insufficient to cover the surface with glycan spokes as required in the scaffold orientation (14). Moreover, the horizontal orientation has the advantage of allowing for continuous polymerization of glycans. Adding glycan hoops, or segments of hoops, leads to elongation of the cylinder without an increase in diameter, a requirement to maintain the rod shape of bacteria like *E. coli* as the cell grows. Importantly, the orientation of glycans in hoops around the cylinder improves the structural strength of the cell wall in the transverse direction where the tension is greatest. These growth and structural advantages would also pertain if the glycan hoops are in actuality spirals with modest pitch, an open experimental question. Previous studies by Boulbitch *et al.* (25) have also shown that the elastic properties of the horizontal model are in good agreement with the experimentally measured anisotropy in the elastic moduli of the *E. coli* cell wall (11). Further studies by Pink *et al.* (26) have noted that a horizontal peptidoglycan network with short glycan strands exhibits an increase in permeability over a network with intact glycan hoops, although they do not explicitly include the physical effects of turgor pressure. Altogether, we conclude that the single-peptidoglycan-layer model with glycans oriented in the hoop-like direction provides a reasonable foundation for addressing the mechanical properties of the *E. coli* cell wall.

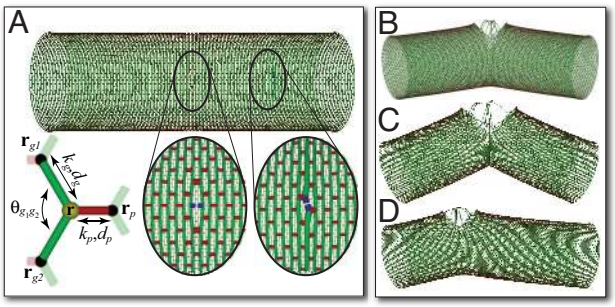

Fig. 1. Elastic model of the peptidoglycan network predicts "cracked" cell shapes. Glycan strands (shown in green) are hoops that wrap around the circumference of the cylinder, whereas peptide crosslinks (shown in red) are longitudinal. Both are under tension due to osmotic pressure. (*A*) The *Left Inset* zooms in on a region of the cell wall without defects and schematically illustrates the elastic forces on each vertex (see Fig. S1 and *Materials and Methods* for more details). The *Center* and *Right Insets* zoom in on regions missing a single peptide or glycan, respectively, shown as broken blue links. The tension in the remaining glycans and peptides relative to a cylinder without defects is represented by the width of the bonds, where the width is doubled in the bond with the maximal increase in tension (≈10%). Around each defect, the increase in stress in the surrounding material is confined to the immediate vicinity of the defect. (*B* and *C*) A patch of defects centered near midcylinder results in a cracked shape (*B*) with the cracking angle closing as the size of the defect patch increases (*C*). (*D*) Off-center defect patches result in an off-center cracked cell shape. The number of defects shown here is identical to that in *B*.

Model Predictions of Cell-Wall Response to Damage. Having formulated a physical model, we next sought to determine how it would respond to perturbation. Specifically, we determined the effect of removing a peptide or glycan from an otherwise perfect lattice. Such defects cause additional strain and increased tension in the surrounding glycans and peptides. In the 3 *Insets* of Fig. 1*A*, we zoom in on regions of a model cell wall (from left to right) with no defect, with a single peptide defect, and with a single glycan defect. In the first case, we specify the relevant quantities used to compute the elastic forces on the peptidoglycan springs, which are described in detail in *Materials and Methods*. In the latter cases, the maximal increase in tension is modest (≈10%) and the perturbations are confined to small neighborhoods around the defects. The short range of perturbation is independent of the size of the network (see Fig. S2) and indicates that nonadjacent defects behave essentially independently.

To test the effects of a local accumulation of cell-wall damage, we began by removing 2 neighboring peptides near midcell. We then successively removed the peptides under the highest degree of tension, resulting in a growing patch of peptide defects near the center of the model cell. As shown in Fig. 1*B* and Fig. S3, the model cell "cracks" around the center, with 2 cylindrical regions angling away from the middle of the patch. The cracking angle in Fig. 1*B* is 165°, and decreases as the size of the patch of peptide defects increases (to 145° in Fig. 1*C*). As shown in Fig. 1*D*, cracking also occurs around off-center patches of defects. The cross-sectional diameter remains nearly constant along the cylindrical portions, with an average value slightly less than the undefected case. The remaining glycan strands spanning the crack are required to approximate the surface of the membrane on which the turgor pressure is acting, but the overall cracked shape is not sensitive to the presence of other glycan defects (see Fig. S5).

***E. coli* Cells Crack Before Lysing When Treated with Vancomycin.** Our model makes 2 specific predictions: (*i*) once enough damage accumulates at a specific location along the cell wall, the cell will crack perpendicular to the longitudinal axis and (*ii*) the strain due to these defects will not propagate far through the peptidoglycan network, so that the regions of the cell away from the crack will maintain their cylindrical shapes with roughly unchanged diameters. To experimentally test these predictions, we used time-lapse microscopy to examine how the peptidoglycan transpeptidation inhibitor vancomycin affects *E. coli* cell shape. The antibiotic vancomycin inhibits cell-wall synthesis by binding to the terminal D-Ala–D-Ala of peptidoglycan precursors, thereby preventing peptide crosslinking of the peptidoglycan

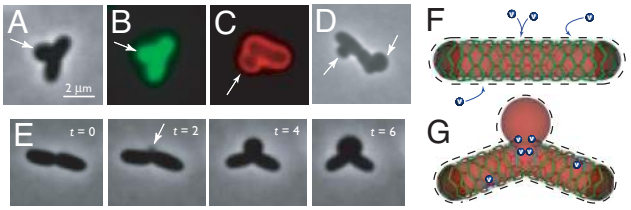

Fig. 2. Bulge formation in *imp4213 E. coli* bacteria in response to vancomycin treatment. (*A*) Phase-contrast image of a typical bulge deformation of an initially rod-shaped cell in response to vancomycin treatment. The bulge (arrow) occurs near midcell, and the cell ''cracks'' around the bulge. (*B*) Fluorescence of cytoplasmic GFP extends into the bulge in the cell in *A*. (*C*) FM4–64 membrane stain of a cell with an off-center bulge. (*D*) Cell with 2 bulges. (*E*) Growth of a bulge at a nascent division site, with images shown at 2-min intervals. Time is measured in minutes, and $t = 0$ is arbitrary. (Scale bar: 2 μm.) (*F* and *G*) Proposed mechanism of bulging: The permeable outer membrane (dashed line) of an *imp4213 E. coli* cell allows the passage into the periplasm of vancomycin (blue discs), which blocks peptide crosslinking of the cell wall (green and red rods). The cell wall cracks into 2 cylindrical regions around the high concentrations of vancomycin-induced peptide defects (broken blue rods) near midcell, and the cytoplasmic membrane (transparent red) bulges out of the crack. The poles of the cell (dark hemispheres) are relatively inert compared to the cylindrical region of the cell, hence vancomycin has little effect in these regions.

network; although vancomycin also blocks glycan chain polymerization *in vitro* (27, 28), the transglycosylase inhibition at the concentration we used (1 μg/ml) is only 3% (29). Vancomycin was therefore an appropriate tool to test our predictions of the effects of peptide defect accumulation on cell shape. A fluorescent derivative of vancomycin has previously been used to label nascent cell wall in the Gram-positive bacterium *Bacillus subtilis* (30, 31). However, in Gram-negative bacteria, like *E. coli*, the outer membrane blocks vancomycin, which has precluded the use of vancomycin to study these cells.

We were able to study the effects of vancomycin on *E. coli* by using an *imp4213* strain that contains a mutation in the outer-membrane protein Imp that perturbs LPS biosynthesis. The resulting increase in outer-membrane permeability allows the passage of a variety of molecules, including vancomycin, that are normally blocked (32, 33). Importantly, the *imp4213* mutation caused no detectable perturbation to growth rate or morphology. We imaged *imp4213* cells after incubation with 1 μg/ml vancomycin. Most cells survived and continued to grow for at least 30 min following addition of vancomycin, after which time damage to the cell wall typically manifested as a bulge on the side of the cell, as shown in Fig. 2. After a bulge formed, cells appeared to ''crack'' around the bulge, with 2 cylindrical regions angling away from the bulge, in the same manner shown in Fig.1 *B–D*. All bulges examined contained cytoplasmic GFP, as illustrated in Fig. 2*B* (see *Materials and Methods*). Although bulges frequently occurred near the middle of the cell (in 180 of 210 cells), bulges were also observed at other locations along the cylindrical region (25 of 210), as shown in Fig. 2*C*. However, no bulges were ever observed at the cell poles. Furthermore, no cells were observed to swell globally, only to form local bulges. Multiple bulges sometimes appeared in a single cell, as shown in Fig. 2*D*, although less frequently than single bulges (5 of 210).

By time-lapse microscopy, we were able to observe the development of these bulges. The time course in Fig. 2*E* shows images taken every 2 min of an *imp4213* cell, in the process of constriction, that developed a bulge at the nascent division site. As the bulge grew larger, the cracking of the cell increased, decreasing the angle between the 2 cylindrical halves. All cells eventually lysed after several hours, although the time interval between the introduction of vancomycin and lysis varied significantly. In every bulged cell whose lysis was observed and whose shape after lysis could be ascertained (24 of 24), the remaining husk of the cell wall clearly retained a cylindrical shape but lost the bulge (see example in Fig. S4*D*), suggesting that the bulge is primarily membrane unenclosed by peptidoglycan so that the bulge is lost upon lysis. Another notable feature of *imp4213* cells after vancomycin treatment is that the regions outside of a bulge retain their cylindrical shapes; the only obvious change in the cell shape, other than the growth of the bulge, is the decrease in the angle between the 2 cylindrical regions (see Fig. S4). In Fig. 2 *F* and *G*, we show schematically our proposed mechanism for bulge formation in cells exposed to vancomycin. In *imp4213 E. coli* cells, the porous outer membrane allows the passage of vancomycin molecules, which prevent peptide crosslinking. As a cell grows in the presence of vancomycin, continued peptidoglycan synthesis introduces peptide defects. The high rate of peptidoglycan synthesis at the nascent division site may create a high concentration of peptide defects at midcell, about which the cell can crack, creating a hole in the cell wall through which the cytoplasmic membrane can expand. The agreement between the predicted and observed cracked cell shapes in Fig.1 *B–D* and Fig. S3 and in Fig. 2 provides strong support for our physical model and suggests that cell-wall defects are likely responsible for the shapes observed in real cells upon treatment with vancomycin.

Robustness of the Shape of Model Cells. The time required for bulges to form and the occasional appearance of multiple bulges following treatment with vancomycin (see Fig. 2*D*) suggest that significant and widespread damage to the cell wall can be sustained without causing loss of shape, until enough local damage accumulates to produce a cytoplasmic bulge. To assess the robustness of the shape of the model cell in Fig. 1*A* to randomly placed cell-wall defects, we computationally introduced successively larger concentrations of peptide defects. In Fig. 3*A*, we show the results of randomly removing 5%, 10%, 20%, or 30% of the peptides, leaving the glycans intact. Because half of the peptides lie out of the plane of the peptidoglycan monolayer and do not contribute to the bearing of osmotic stress in our model, an additional 30% defect concentration is equivalent to 35% total crosslinking, which approaches the lower limit for *E. coli* viability (23, 34).

Experimentally, the length distribution of glycan strands in the *E. coli* cell wall is found to peak at ≈5–10 disaccharide units with most strands <30 units (7, 35), indicating that the hoops in our model are likely composed of many short strands separated by missing glycans. To bring our model into closer contact with experiment, we used Monte Carlo simulations to position glycan defects within model cell walls to reproduce the observed length distribution from ref. 35. (this procedure results in the removal of ≈10% of the glycan springs; see SI). In Fig. 3*B*, we show the results of randomly removing 0%, 5%, 10%, or 20% of the peptides while maintaining the observed glycan strand-length distribution. In Fig. 3*C*, we demonstrate the good agreement between the glycan strand length distribution of the model cell wall in the first panel of Fig. 3*B* and experimental measurements.

In Fig. 3 *A* and *B*, the cell wall relaxes to a predominantly cylindrical shape, with local deformations in areas of high defect density. At the higher defect concentrations some slight overall bending is also observed. As the peptide defect concentration increases, the length of the cylinder increases roughly linearly until high defect concentrations are reached, while removing 10% of the glycan springs slightly increases the cylinder radius, similar to the effects of increasing the osmotic pressure differential across the cytoplasmic membrane (see Fig. S6). The presence of defects transforms the regular grid in Fig. 1*A* into a more random pattern, but one that on average preserves the circumferential direction of the glycan strands.

In addition to bearing the stress of osmotic pressure, the cell wall must also be porous to allow the passage of nutrients,

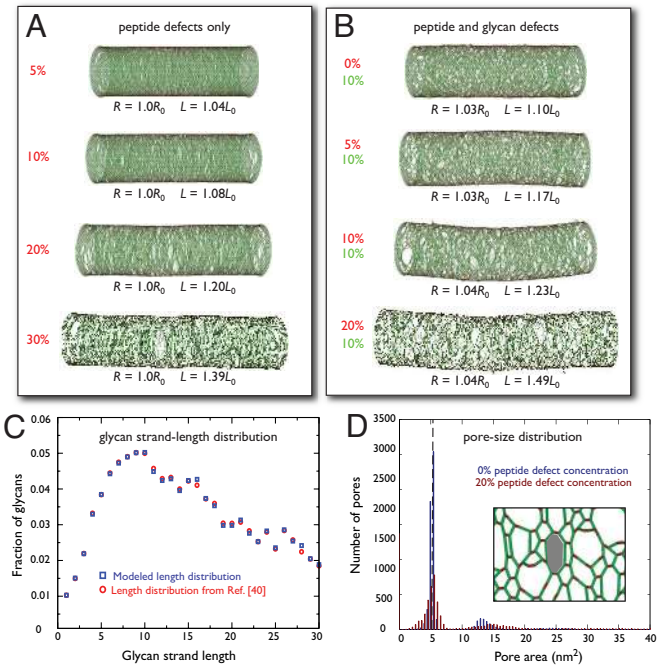

Fig. 3. Robustness of the shape of a model cell with peptidoglycan defects. (*A* and *B*) Upon removal of an increasing concentration of randomly chosen peptide bonds (*A*) or peptide and glycan bonds (*B*), the cell wall maintains an approximately cylindrical shape, with slightly increased dimensions as indicated. The peptide and glycan defect concentrations are shown as percentages in red and green, respectively. The radii, lengths, and defect concentrations are measured relative to a single-layer cell wall with radius R_0 and length L_0. In *B*, the defects are chosen so that the glycan strand-length distribution matches the experimental distribution from ref. 35. (*C*) Comparison of the computed strand-length distribution of the topmost image in *B* with the experimental distribution. (*D*) The glycan defects in *B* create large pores in the cell wall; shown are the distributions of pore areas in the topmost and bottom images.

proteins, and even nucleic acids during transformation (36, 37). For a perfect network without defects, the peptidoglyan is tiled with hexagonal "tesserae" or pores composed of 2 peptide crosslinks and 4 disaccharide glycan units with a small, uniform pore size (roughly 5 nm^2 for l_p = 1 nm; see, e.g., Fig. 1*A Insets*). However, previous studies have noted the increase in porosity caused by peptidoglycan defects (26), which link adjacent pores to create new pores with more edges and larger area. In Fig. 3*D*, we show a histogram of the tessera area distribution for the model cell walls in the topmost and bottom images of Fig. 3*B* with 0 and 20% peptide defect concentrations, respectively. The presence of glycan defects alone (blue distribution) creates pores larger than the uniform pore area in a perfect network (indicated by the dashed line). Adding peptide defects creates both larger and smaller pores, since the osmotic pressure simultaneously enlarges pores with more edges and shrinks the surrounding material if it lacks defects. For example, see Fig. 3*D Inset*, showing a region of the network in the third image from the top in Fig. 3*B*. There is an expanded decagonal pore, shown shaded in gray, formed by the removal of a glycan spring, but also a contracted hexagonal pore in the lower left corner. Comparing the distributions of pore sizes in Fig. 3*D*, the main effect of increasing the peptide defect concentration from 0 to 20% is to increase the number of pores with large areas, with small numbers of pores as large as 400 nm^2.

Cell-Shape Variants. To date, consideration of how peptidoglycan organization produces different cell shapes has focused on

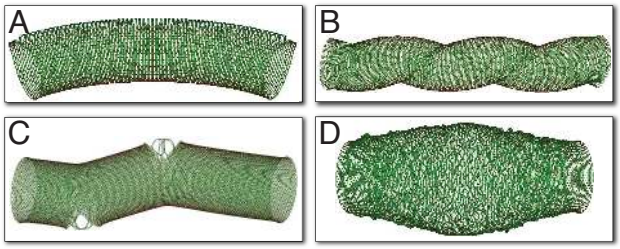

Fig. 4. Common bacterial cell shapes generated via defects in a model cylindrical cell wall. (*A*) Removal of peptide bonds along the top surface of the cylinder results in a curved cell shape reminiscent of *Caulobacter crescentus*. (*B*) A reduction in the relaxed lengths of peptides and glycans along a helical path generates a helical cell shape similar to that of spirochaetes or the bacterium *Helicobacter pylori*. (*C*) Removal of 2 patches of peptide defects on opposite sides of the cylinder, separated by half the cylinder length, creates a snakelike cell shape similar to vancomycin-treated *E. coli* cells with multiple bulges. (*D*) Increased substitution of glycan–peptide–glycan segments in place of glycans near the midplane of the cell creates a swelled cylinder, similar to the lemon shape of cylindrical Gram-negative bacteria after treatment with the MreB inhibitor A22.

patterns of peptidoglycan insertion. However, since the peptidoglycan network appears capable of tolerating a large number of defects, we decided to explore the possibility that specific patterns of defects could induce specific cell shapes. We noticed that the bending of the cylinders in Figs. 1 and 3 is reminiscent of the flexing of an elastic tube. For such a tube, certain deformations (modes) require less energy than others to excite to a given amplitude. Indeed, the most flexible mode of a peptidoglycan network similar to the one in Fig. 1*A* is a bend mode (Fig. S7*A*). Although a single peptide defect causes little change to local shape, such a defect near midcell does contribute to this bend mode. In principle, the accumulation of bend from multiple peptide defects could produce a large change in the global cell shape. The next most flexible mode is a twist mode (Fig. S7*B*). By symmetry, a single peptide defect does not produce twist. However, a glycan defect at midcell produces both bend and twist.

Guided by the correspondence of peptide defects with bending and glycan defects with twisting, we modified our model cell with collections of defects designed to produce specific shapes. Introducing lines of peptide defects along 1 side of the cell resulted in a large amplitude bend, as shown in Fig. 4*A*. The resulting cell wall resembles the Gram-negative bacterium *C. crescentus*. This result prompted us to ask whether other common bacterial cell shapes could also be produced by local modifications of the cell wall. Thus far, we have considered only the removal of peptides or glycans, but a wider class of defects consisting of spatially varying spring constants or spring lengths is both biologically relevant, e.g., via changes in chemical crosslinking (3), and accessible within our model. In particular, upon shortening by 75% the relaxed lengths of the peptidoglycan springs along a helical path winding around the cylinder, the cell relaxes into the helical shape shown in Fig. 4*B*, resembling spirochaetes or the bacterium *Helicobacter pylori*. The removal of 2 patches of peptide defects on opposite sides of the cylinder, separated by half the cylinder length, leads to a snakelike cell shape as shown in Fig. 4*C*. In all these cases, the observed changes in cell shape result from a small number of changes to the peptidoglycan network, demonstrating that with subtle patterning, the same basic peptidoglycan network can produce many shapes.

In addition to explaining species-specific shape differences, our model can also be used to explore chemically-induced shapes changes. For example, treatment of Gram-negative bacteria with the chemical A22 (38), an inhibitor of the cytoskeletal protein MreB, often results in lemon-shaped cells. A similar shape

change is seen in Fig. 4*D*, where glycan springs were randomly replaced by an effective spring representing a glycan–peptide–glycan segment. These effective springs mimic the results of misdirected glycan synthesis along the longitudinal axis of the cell, which ultimately incorporates peptide crosslinks into the circumferential hoops (Fig. S8). The frequency of replacement is higher near midcell, where more new peptidoglycan synthesis takes place (39). The similarity between the model cell walls in Fig. 4 and common bacterial cell shapes demonstrates the possibility of cell shape variants via simple peptidoglycan modifications, and also predicts specific mechanisms through which they might be achieved.

Discussion

Although it is widely recognized that cell shape plays a critical role in regulating cellular functions in bacteria, the molecular mechanisms and structures that determine cell shape are not well understood. To quantitatively investigate possible mechanisms for cell-shape determination, we developed a simple elastic model of the Gram-negative cell wall in which the peptidoglycan subunits are represented as springs that balance the cell's osmotic pressure. Within this model, a cracked cell shape resulted from a patch of peptide defects (Fig. 1), even in the background of a realistic glycan strand-length distribution (Fig. S5). In confirmation of this prediction, we found that *E. coli imp4213* mutants exposed to vancomycin underwent a regular pattern of cell-shape deformation: after a period of growth, 1 bulge or sometimes multiple bulges appeared on the side of each cell, and cells often cracked around the bulges. The angle of cracking progressed over time, but the 2 regions on either side of the bulge remained cylindrical even when the crack angle reached ≈90°.

Importantly, bulging has been observed after inhibition of peptidoglycan synthesis either at precursor synthesis or late in assembly (40). Midcell bulging and lysis also occurs when an inactive peptidoglycan synthesis is overexpressed (41). In support of our proposed mechanism in Fig. 2 *F* and *G*, lysis can be relieved in multiple-hydrolase-mutant strains. We have also observed bulging and lysis in *C. crescentus* cells, which are naturally sensitive to vancomycin (data not shown). Cracking and membrane bulging at other locations along the side of the cylinder can also occur if a high concentration of peptide defects develops, but are unlikely to occur at the relatively inert poles where little or no peptidoglycan synthesis takes place.

Using our elastic model, we found that the cylindrical shape of the cell wall is robust to large concentrations of both peptide and glycan defects. However, these defects increase the size of the pores in the cell wall, allowing for the diffusive passage of nutrients, waste products, and other large molecules such as DNA. We also found that a small concentration of ordered defects can produce a variety of cell shapes, including crescent-shaped, helical, and lemon-shaped cells. Because defects cause only a local increase in tension (see Fig. 1*A* and Fig. S2), the defect-induced changes in cell shape in Figs. 1, 3, and 4 are unlikely to be qualitatively affected by a small average global helicity in the glycan strand orientation, especially with a realistic glycan strand-length distribution.

The robustness of our model cells to defects and the experiments with vancomycin-treated cells suggest that cells can tolerate a significant concentration of peptidoglycan defects. Indeed, this robustness to defects is a general property of 2D spring networks (26). Taken together, our results suggest that "make-before-break" synthesis of peptidoglycan may not be absolutely necessary. As long as only moderate breaking occurs before making, the peptidoglycan network may retain its shape and integrity. This allows some imprecision in the synthesis of new peptidoglycan, and allows for the maintenance of the rod-shaped morphology even at low peptidoglycan density (23).

In addition to cracked cells, many common variants of rod-shaped cells, such as crescent-shaped, helical, snake-like, and lemon-shaped cells, can be obtained by small perturbations of the model peptidoglycan network. The fact that isolated cell walls (sacculi) retain the shape of the intact cell (11, 13) indicates that inhomogeneous synthesis or processing of peptidoglycan during growth is sufficient to create shape variants. In many cases, these shapes reflect the normal modes of the network (Fig. S7); that is, they are the "easiest" shapes to make by perturbing a cylinder. One key difference between rod-shaped, ellipsoidal, and round bacteria is the organization of the peptidoglycan synthesis enzymes (for a review, see ref. 3). Our model suggests that the lemon-shaped cells that result from A22 treatment could be due to a disruption in the normal synthesis of glycan hoops, leading to misoriented glycan strands. In *C. crescentus*, a single intermediate-filament-like protein, crescentin, is localized to the cell's inner curvature and is both necessary and sufficient to produce a curved cell shape (42). Our model suggests that crescentin might function by selectively stabilizing peptide bonds on one side of the cell surface. There are other related defect patterns that produce similar shapes, e.g., in the second image from the top in Fig. 3*B* bending is caused by an uneven distribution of peptide defects. The cell walls in Fig. 4 are intended to demonstrate that relatively small changes to the peptidoglycan can lead to large changes in shape, and that these changes could potentially reflect spatially dependent regulation of synthesis. The conserved molecular structure of peptidoglycan suggests that it might be possible to force one bacterium to adopt the shape of a different bacterium simply by expressing the factors responsible for establishing and maintaining a particular class of peptidoglycan inhomogeneities.

Although *E. coli* cells maintain a rod shape during exponential growth, they are also able to adopt a wide variety of shapes in the face of environmental, chemical, or genetic perturbations. Since the molecular structure of peptidoglycan is conserved in bacteria, the dependence of cell shape on the cell wall is likely similar in all Gram-negative bacteria. In this work, we have introduced a model for the Gram-negative cell wall that makes predictions about mechanisms for cell-shape determination via peptidoglycan organization. Work in progress includes integrating our current model with a description of the cytoplasmic membrane mechanics and of nonlinear elastic effects to study *in vivo* cell-shape determination, and growth of multilayer cell walls. Future experimental work will not only probe these mechanisms in natural bacterial cell-shape selection, but may also directly exploit these mechanisms to synthetically alter bacterial cell shapes.

Materials and Methods

Spring Model of Gram-Negative Cell Wall. We model the peptidoglycan cell wall of a Gram-negative rod-shaped bacterium such as *E. coli* as a single-layered cylindrical spring network, as shown, e.g., in Fig. 1 and in expanded view in Fig. S1. In the absence of defects, the network consists of N_h circular peptidoglycan strands around the circumference of the cylinder, each consisting of N_g individual glycan springs. Adjacent glycan strands are crosslinked by peptides between alternating pairs of glycan springs (see Fig. 1*A*). Therefore, the vertices of the network occur where 2 glycan springs and a peptide spring meet. In most cases, we studied a cylinder composed of $N_h = 150$ glycan strands, each composed of $N_g = 100$ glycan springs. In the absence of defects these model cells have a length/diameter ratio of ≈3:1, similar to a rod-shaped *E. coli* cell. The exceptions are in Fig 4 *B* and *C*, where we elongated the cell to $N_h = 300$ and 200, respectively, and Fig. 4*A*, where the cell is composed of $N_h = 130$ glycan strands of $N_g = 60$ springs.

In our model, the relatively unstretchable glycans and relatively stretchable peptides are represented as springs with relaxed lengths l_g and l_p, respectively, and spring constants k_g and k_p, respectively, with $k_g \gg k_p$. A brief summary of the forces acting on the peptidoglycan follows, and more details regarding the calculation of forces can be found in the SI. For the vertex at $\mathbf{r}$, connected to vertices at $\mathbf{r}_{g1}$ and $\mathbf{r}_{g2}$ via glycans and to the vertex $\mathbf{r}_p$ via a peptide, the total spring extension force $\mathbf{F}_k(\mathbf{r})$ is a sum of 3 Hookean forces. To model the

tendency of glycans to form straight strands in the absence of crosslinking, we also include the force due to glycan bending, with force constant κ_{gg}. Finally, the force due to osmotic pressure differential Π across the cytoplasmic membrane is $\mathbf{F}_{\Pi}(\mathbf{r}) = \Pi\nabla V$, where V is the volume of the cylinder and Π is the gradient with respect to the vertex position $\mathbf{r}$. The total force on the vertex at $\mathbf{r}$ is therefore $\mathbf{F}(\mathbf{r}) = \mathbf{F}_{\Pi} + \mathbf{F}_k + \mathbf{F}_{\text{bend}}$. Electrostatic charges will be efficiently screened by ions in the aqueous medium, except at very short length scales. A previous study of electrostatic fluctuations of a small, flat patch of peptidoglycan used a Debye shielding length of 0.3 nm, reflecting the strong screening of charges (11). Therefore, we have ignored electrostatic forces, which would amount to at most a modest rescaling of the spring constants in our model.

Defects are treated as virtual springs with $k = 0$ for the purposes of defining the edges of the hexagons. The ends of the cylinder are treated as an N_g-gon, subdivided as above into triangles to calculate the force due to osmotic pressure acting on the vertices at the ends of the cylinder. To determine the equilibrium configuration of the network, we use a steepest descent algorithm until the average force acting on the vertices is $<2 \times 10^{-4} k_p l_p$ in magnitude.

We measure all distances in units of the relaxed peptide length l_p, and all forces in units of $k_p l_p$. The osmotic pressure is then measured in units of k_p/l_p. We modeled the glycan springs with $k_g = 5k_p$ and $l_g = 2l_p$ (except as noted for the defects in Fig. 4*B*) and with bending spring constants $\kappa_{gg} = 10$ pN nm and $\kappa_{pg} = 0$. We have assumed an internal osmotic pressure of $\Pi = 0.01$ to roughly match realistic pressures in bacteria, although we note that our qualitative observations hold over a large range of Π. With $k_p \approx 10^{-2}$ N/m and $l_p \approx 1$ nm, $\Pi \approx 1$ atm, and a rough estimate of the Young's modulus is 30 MPa (25), which lies within the range of AFM measurements between 25 and 45 MPa, depending on orientation of the cell wall relative to the substrate (11). The glycan strand persistence length is ≈10 nm, matching experimental estimates (43). Our estimates are meant to demonstrate that the parameters in our model approximate the bulk elastic properties of the sacculus, and are therefore adequate for our intended level of description of the cell wall. Moreover, our qualitative results are robust to changes in the Young's modulus and glycan strand persistence length caused by variations in k_p, l_p, and κ_{gg}.

Experimental Methods. All experiments were performed on the previously-described vancomycin-sensitive strain *E. coli imp4213* (44). Cells used for imaging were grown to log phase ($OD_{600} = 0.5–0.8$) in LB medium. Live-cell time-lapse experiments were performed by pipetting untreated exponentially growing cells onto a 1% agarose pad made with LB and a final concentration of 1 μg/ml vancomycin-hydrochloride (Sigma–Aldrich) and imaging the cells every 2 min. The presence of cytoplasm in the cell bulges was observed by introducing into *imp4213* the pZS21-GFP plasmid (gift of the laboratory of Tom Silhavy, Princeton University, Princeton, NJ) that constitutively expresses cytoplasmic GFP. Cell membranes were visualized by adding membrane dye FM 4-64 (Molecular Probes) to the agarose pad to a final concentration of 2 μg/ml. All images were captured with a Nikon 90i microscope and Rolera-XR cooled CCD camera (Qimaging) using NIS-Elements software (Nikon). In total, 210 cells were observed in time-lapse images and their bulge locations were recorded.

ACKNOWLEDGMENTS. We thank Hernan Garcia, Tom Silhavy, Tristan Ursell, and Tiffany Vora for insightful discussions; Natacha Ruiz (Princeton University, Princeton, NJ) for providing the *imp4213 E. coli* strain; Juliana Malinverni (Princeton University, Princeton, NJ) for providing the pZS21-GFP plasmid; Jonathan Guberman for assistance in quantifying the image data; Eleni Katifori for providing the volume calculation algorithm; and John Rittenhouse for contributions to modeling. This work was funded in part by National Institutes of Health Grants K25 GM075000 and R01 GM073186.

1. Cabeen MT, Jacobs-Wagner C (2005) Bacterial cell shape. *Nat Rev Microbiol* 3:601–610.
2. Höltje JV (1998) Growth of the stress-bearing and shape-maintaining murein sacculus of *Escherichia coli*. *Microbiol Mol Biol Rev* 62:181–203.
3. Scheffers DJ, Pinho MG (2005) Bacterial cell wall synthesis: New insights from localization studies. *Microbiol Mol Biol Rev* 69:585–607.
4. Young KD (2006) The selective value of bacterial shape. *Microbiol Mol Biol Rev* 70:660–703.
5. Matias VRF, Al-Amoudi A, Dubochet J, Beveridge TJ (2003) Cryo-transmission electron microscopy of frozen-hydrated sections of *Escherichia coli* and *Pseudomonas aeruginosa*. *J Bacteriol* 185:6112–6118.
6. Glauner B, Höltje JV (1990) Growth pattern of the murein sacculus of *Escherichia coli*. *J Biol Chem* 265:18988–18996.
7. Harz H, Burgdorf K, Höltje JV (1990) Isolation and separation of the glycan strands from murein of *Escherichia coli* by reversed-phase high-performance liquid chromatography. *Anal Biochem* 190:120–128.
8. Glauner B, Höltje JV, Schwarz U (1988) The composition of the murein of *Escherichia coli*. *J Biol Chem* 263:10088–10095.
9. Koch AL (2000) Simulation of the conformation of the murein fabric: The oligoglycan, penta-muropeptide, and crosslinked nona-muropeptide. *Arch Microbiol* 174:429–439.
10. Meroueh SO, *et al.* (2006) Three-dimensional structure of the bacterial cell wall peptidoglycan. *Proc Nat Acad Sci USA* 103:4404–4409.
11. Yao X, Jericho M, Pink D, Beveridge T (1999) Thickness and elasticity of Gram-negative murein sacculi measured by atomic force microscopy. *J Bacteriol* 181:6865–6875.
12. Labischinski H, Goodell EW, Goodell A, Hochberg ML (1991) Direct proof of a ''more-than-single-layered'' peptidoglycan architecture of *Escherichia coli* W7: A neutron small-angle scattering study. *J Bacteriol* 173:751–756.
13. Gan L, Chen S, Jensen GJ (2008) Molecular organization of Gram-negative peptidoglycan. *Proc Nat Acad Sci USA*.
14. Vollmer W, Höltje JV (2004) The architecture of the murein (peptidoglycan) in Gram-negative bacteria: Vertical scaffold or horizontal layer(s)? *J Bacteriol* 186:5978–5987.
15. Trueba FJ, Woldringh CL (1980) Changes in cell diameter during the division cycle of *Escherichia coli*. *J Bacteriol* 142:869–878.
16. Vinella D, Joseleau-Petit D, Thévenet D, Bouloc P, D'Ari R (1993) Penicillin-binding protein 2 inactivation in *Escherichia coli* results in cell division inhibition, which is relieved by FtsZ overexpression. *J Bacteriol* 175:6704–6710.
17. Nilsen T, Ghosh AS, Goldberg MB, Young KD (2004) Branching sites and morphological abnormalities behave as ectopic poles in shape-defective *Escherichia coli*. *Mol Microbiol* 52:1045–1054.
18. de Pedro MA, Young KD, Höltje JV, Schwarz H (2003) Branching of *Escherichia coli* cells arises from multiple sites of inert peptidoglycan. *J Bacteriol* 185:1147–1152.
19. Lange R, Hengge-Aronis R (1991) Growth phase-regulated expression of *bolA* and morphology of stationary-phase *Escherichia coli* cells are controlled by the novel sigma factor σ^S. *J Bacteriol* 173:4474–4481.
20. Takeuchi S, DiLuzio WR, Weibel DB, Whitesides GM (2005) Controlling the shape of filamentous cells of *Escherichia coli*. *Nano Lett* 5:1819–1823.
21. Höltje JV, Heidrich C (2001) Enzymology of elongation and constriction of the murein sacculus of *Escherichia coli*. *Biochimie* 83:103–108.
22. Koch AL (1985) How bacteria grow and divide in spite of internal hydrostatic pressure. *Can J Microbiol* 31:1071–1084.
23. Prats R, de Pedro MA (1989) Normal growth and division of *Escherichia coli* with a reduced amount of murein. *J Bacteriol* 171:3740–3745.
24. Dmitriev B, Toukach F, Ehlers S (2005) Towards a comprehensive view of the bacterial cell wall. *Trends Microbiol* 13:569–574.
25. Boulbitch A, Quinn B, Pink D (2000) Elasticity of the rod-shaped Gram-negative eubacteria. *Phys Rev Lett* 85:5246–5249.
26. Pink D, Moeller J, Quinn B, Jericho M, Beveridge T (2000) On the architecture of the Gram-negative bacterial murein sacculus. *J Bacteriol* 182:5925–5930.
27. Anderson JS, Matsuhashi M, Haskin MA, Strominger JL (1967) Biosynthesis of the peptidoglycan of bacterial cell walls. *J Biol Chem* 242:3180–3190.
28. Reynolds PE (1989) Structure, biochemistry and mechanism of action of glycopeptide antibiotics. *Eur J Clin Microbiol Infect Dis* 8:943–950.
29. van Heijenoort Y, Derrien M, van Heijenoort J (1978) Polymerization by transglycosylation in the biosynthesis of the peptidoglycan of *Escherichia coli* K 12 and its inhibition by antibiotics. *FEBS Lett* 89:141–144.
30. Daniel RA, Errington J (2003) Control of cell morphogenesis in bacteria: Two distinct ways to make a rod-shaped cell. *Cell* 113:767–776.
31. Tiyanont K, *et al.* (2006) Imaging peptidoglycan biosynthesis in *Bacillus subtilis* with fluorescent antibiotics. *Proc Nat Acad Sci USA* 103:11033–11038.
32. Wu T, *et al.* (2005) Identification of a multicomponent complex required for outer membrane biogenesis in *Escherichia coli*. *Cell* 121:235–245.
33. Ruiz N, Falcone B, Kahne D, Silhavy TJ (2005) A genetic strategy to probe organelle assembly. *Cell* 121:307–317.
34. de Jonge BLM, *et al.* (1989) Peptidoglycan synthesis during the cell cycle of *Escherichia coli*: Composition and mode of insertion. *J Bacteriol* 171:5783–5794.
35. Obermann W, Höltje JV (1994) Alterations of murein structure and of penicillin-binding proteins in minicells from *Escherichia coli*. *Microbiology* 140:79–87.
36. Beveridge TJ (1999) Structures of Gram-negative cell walls and their derived membrane vesicles. *J Bacteriol* 181:4725–4733.
37. Demchick P, Koch AL (1996) The permeability of the wall fabric of *Escherichia coli* and *Bacillus subtilis*. *J Bacteriol* 178:768–773.
38. Gitai Z, Dye NA, Reisenauer A, Wachi M, Shapiro L (2005) MreB actin-mediated segregation of a specific region of a bacterial chromosome. *Cell* 120:329–341.
39. Aaron M, *et al.* (2007) The tubulin homologue FtsZ contributes to cell elongation by guiding cell wall precursor synthesis in *Caulobacter crescentus*. *Mol Microbiol* 64:938–952.
40. Goodell EW, Lopez R, Tomasz A (1976) Suppression of lytic effect of beta lactams on *Escherichia coli* and other bacteria. *Proc Natl Acad Sci USA* 73:3293–3297.
41. Meisel U, Höltje JV, Vollmer W (2003) Overproduction of inactive variants of the murein synthase PBP1B causes lysis in *Escherichia coli*. *J Bacteriol* 185:5342–5348.
42. Ausmees N, Kuhn JR, Jacobs-Wagner C (2003) The bacterial cytoskeleton: An intermediate filament-like function in cell shape. *Cell* 115:705–713.
43. Cros S, Garnier C, Axelos MAV, Imberty A, Pérez S (1996) Solution conformations of pectin polysaccharides: Determination of chain characteristics by small angle neutron scattering, viscometry, and molecular modeling. *Biopolymers* 39:339–352.
44. Eggert US, *et al.* (2001) Genetic basis for activity differences between vancomycin and glycolipid derivatives of vancomycin. *Science* 294:361–364.